*Journal of Alloys and Compounds, 185* (1992) 7–17
*JALCOM 157*



# Some physical properties of $Zr_2CuH_{4.2}$ in relation to those observed for other $MoSi_2$-type hydrides

R. C. Bowman Jr.
*Aerojet Electronics System Division, PO Box 296, Azusa, CA 91702 (USA)*

J. S. Cantrell
*Department of Chemistry, Miami University, Oxford, OH 45056 (USA)*

A. J. Maeland
*Concrete Solutions, PO Box 1842, Meriden, CT 06450 (USA)*

A. Attalla and G. C. Abell
*EG&G Mound Applied Technologies, Miamisburg, OH 45343-0987 (USA)*

(Received May 23, 1991; accepted in final form October 28, 1991)

## Abstract

The intermetallic compound $Zr_2Cu$ with the tetragonal $MoSi_2$-type structure produces a metastable ternary hydride $Zr_2CuH_x$. Powder X-ray diffraction indicated a monoclinic unit cell for this phase when $x \approx 4.2$. Nuclear magnetic resonance of the proton rotating frame relaxation times gave an activation energy of 0.28 eV for hydrogen diffusion in $Zr_2CuH_{4.2}$. Irreversible changes in the proton relaxation times were noted after the $Zr_2CuH_{4.2}$ sample had been heated above 500 K. X-ray diffraction confirmed the decomposition of the original ternary phase into a mixture of $ZrH_x$ and other components, including metallic copper.

## 1. Introduction

Several $A_2B$ intermetallic compounds with the tetragonal $MoSi_2$-type crystal structure have been found [1] to react wtih hydrogen. Although $Zr_2Cu$ and $Ti_2Cu$ undergo decomposition during reactions with hydrogen above 500 °C [2, 3] to form mixtures of the binary hydrides $ZrH_x$ and $TiH_x$ respectively with copper-rich phases, ternary hydrides $Zr_2CuH_{4.3}$ and $Ti_2CuH_{2.8}$ have been produced [4] when samples were exposed at room temperature to a hydrogen pressure around 1 atm. Additional information on the crystal structures, hydrogen diffusion behavior, thermal stability and disproportionation behavior of $Ti_2CuH_x$ has been previously reported [5, 6]. There have also been several studies on the formation and properties of the ternary hydrides formed by the isomorphous compounds $Ti_2Pd$ [3, 7] and $Zr_2Pd$ [1, 8–10]. The intent of the present paper is to describe the properties of $Zr_2CuH_{4.2}$ as deduced from powder X-ray diffraction, proton nuclear magnetic resonance (NMR) and differential thermal analysis measurements.

0925-8388/92/$5.00

## 2. Experimental details

The $Zr_2Cu$ intermetallic was prepared by arc melting appropriate amounts of zirconium and copper under an argon atmosphere. The purities of the metals were 99.9% copper and 99.95% zirconium. The resulting button was remelted four times to ensure homogeneity. The lattice parameters from its powder X-ray pattern were in good agreement with the published values [11] for $Zr_2Cu$.

The hydride samples were produced from the reaction between the single phase $Zr_2Cu$ and hydrogen gas introduced into the reactor without external heating [4]. The amount of hydrogen absorbed was calculated from the difference between initial and final hydrogen pressures. The charged samples were generally handled in argon-filled glove-boxes.

The X-ray diffraction (XRD) experiments were by means of automated step scans. The primary instrument employed for this work was a Rigaku horizontal, wide angle, automated diffractometer equipped with a 12 kW rotating anode generator. The scans were performed with the generator operating at 40 kV and 80 mA for a copper anode. A 1° dispersion slit, a 0.15 mm (about 0.05°) receiving slit and a 1° scatter slit collectively defined the X-ray beams. A nickel foil filter was placed in the diffracted beam to reduce the Cu K$\beta$ radiation. Scans were performed in 0.05° steps with 0.4 s counts per step. The XRD samples were prepared in a glove-box by mounting the $Zr_2CuH_{4.2}$ powder on a microscope slide with double-sided tape and covering the adhering powder with a thin plastic film. An internal reference standard of NBS silicon (No. 640a) powder was used. XRD pattern analysis was conducted using a DEC PDP-11/44 computer at EG&G Mound and the software SPECPLOT [12] for display, peak location (*i.e.* peak maximum or peak centroid algorithms) and calculated pattern overlay and LATTICE [13] for peak indexing and least-squares lattice pattern determination. Phase determination, unit cell parameters and error analysis were achieved with these two programs.

A Bruker transient NMR spectrometer [5, 8] was used to measure the proton spin–lattice ($T_1$) and rotating frame ($T_{1\rho}$) relaxation times. The proton resonance frequency was 34.5 MHz and the spin-locking magnetic field ($H_1$) was 7.3 G. The $Zr_2CuH_{4.2}$ NMR sample had been flame sealed in an evacuated glass tube of 7 mm outer diameter.

## 3. Structure and hydrogen site occupancy

The structure of the $Zr_2Cu$ intermetallic with its b.c.t. unit cell is shown in Fig. 1. Six interstitial sites that are available for hydrogen occupancy are also indicated in this figure. The nature and symmetry of these sites are summarized in Table 1. Previous NMR measurements of the rigid lattice proton second moments [5, 9] and inelastic neutron-scattering measurements of the hydrogen vibration spectra [1, 10] indicated that only tetrahedral $T_a$

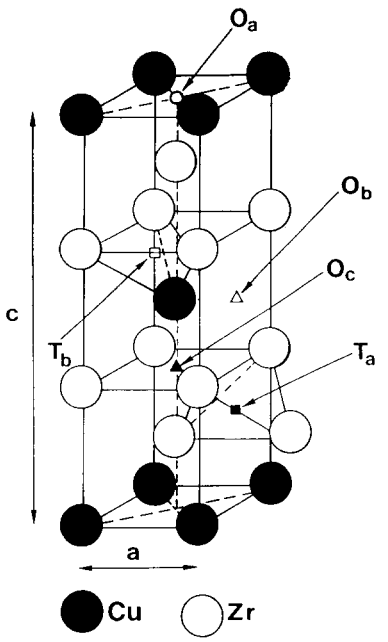


Fig. 1. Crystal structure of $Zr_2Cu$ with potential hydrogen sites.

TABLE 1

Sites for potential hydrogen occupancy in the structure of $Zr_2Cu$

| Label | Position | Site symmetry | Nearest neighbor coordination |
|---|---|---|---|
| $O_a$ | 2b | 4/*mmm* | $Zr_2Cu_4$ |
| $O_c$ | 4e | 4*mm* | $Zr_5Cu$ |
| $O_b$ | 4c | *mmm* | $Zr_4Cu_2$ |
| $T_c$ | 8g | *mm* | $Zr_2Cu_2$ |
| $T_b$ | 16n | *m* | $Zr_3Cu$ |
| $T_a$ | 4d | 4*m*2 | $Zr_4$ |

sites are occupied in $Ti_2CuH_x$ and $Zr_2PdH_x$ when $x<2$. These results have been substantiated by powder neutron diffraction experiments on $Zr_2PdD_{1.7}$ [14] and $Ti_2CuD_{2.0}$ [15]. Since complete occupancy of the $T_a$ sites occurs at $x=2.0$, $A_2BH_x$ hydrides with $x>2$ (*e.g.* $Zr_2CuH_{4.2}$) must have H atoms in one or more of the other sites listed in Table 1. From the earlier studies involving the proton second moments and inelastic neutron scattering on hydrides and neutron diffraction patterns from deuterides [14, 15] for $Ti_2CuH(D)_x$ and $Zr_2PdH(D)_x$ with $x>2$, the most likely candidates are the octahedral $O_b$ (*e.g.* $Zr_4Cu_2$) and $O_c$ (*e.g.* $Zr_5Cu$) and tetrahedral $T_b$ (*e.g.* $Zr_3Cu$) sites for $Zr_2CuH_{4.2}$.

The XRD pattern obtained from an unheated (*i.e.* as-prepared) $Zr_2CuH_{4.2}$ sample is presented in Fig. 2. From a least-squares analysis [13] of the most prominent lines, which are summarized in Table 2, a good fit was obtained for a single phase with a monoclinic unit cell and parameters $a = 0.5635(5)$ nm, $b = 0.5401(4)$ nm, $c = 0.4605(5)$ nm and $\beta = 97.4(2)°$. The errors in the last significant digits are shown in parentheses. Analyses of powder XRD data for two other preparations of $Zr_2CuH_x$ with $x \approx 4.2$ also indicated monoclinic unit cells with similar lattice constants and a $\beta$ angle ranging between 102° and 97°. From a comparison between unit cell volume and $\beta$

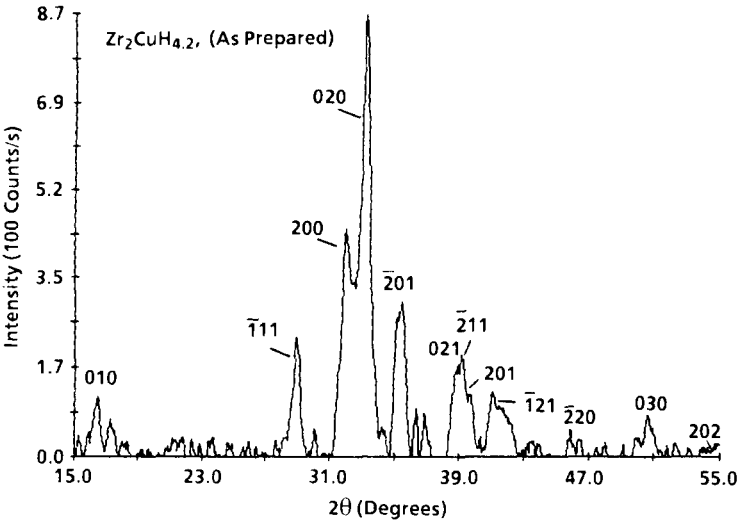


Fig. 2. X-ray diffraction pattern for as-prepared $Zr_2CuH_{4.2}$ obtained with Cu K$\alpha$ radiation.

TABLE 2

Comparison of the X-ray diffraction patterns for monoclinic $Zr_2CuH_{4.2}$ and orthorhombic $Zr_2PdH_{3.4}$ obtained with Cu K$\alpha$ radiation ($\lambda = 0.1542$ nm)

| Monoclinic $Zr_2CuH_{4.2}$ | | | | | Orthorhombic $Zr_2PdH_{3.4}$ | | | |
|---|---|---|---|---|---|---|---|---|
| *h k l* | $2\theta_{obs}$ (deg) | $d_{obs}$ (Å) | $d_{calc}$ (Å) | $I_{rel}$ | *h k l* | $2\theta_{obs}$ (deg) | $d_{obs}$ (Å) | $I_{rel}$ |
| 010 | 16.40 | 5.405 | 5.402 | 12 | 002 | 15.52 | 5.710 | 15 |
| $\bar{1}11$ | 28.90 | 3.089 | 3.085 | 23 | 004 | 31.33 | 2.855 | 11 |
| 200 | 32.00 | 2.797 | 2.798 | 50 | 013 | 35.21 | 2.549 | 18 |
| 020 | 33.20 | 2.698 | 2.701 | 100 | 103 | 35.40 | 2.536 | 40 |
| $\bar{2}01$ | 35.50 | 2.529 | 2.537 | 36 | 110 | 37.23 | 2.415 | 100 |
| $\bar{2}11$ | 39.20 | 2.298 | 2.296 | 20 | 014 | 41.13 | 2.195 | 20 |
| $\bar{1}21$ | 41.05 | 2.199 | 2.193 | 21 | 104 | 41.29 | 2.186 | 12 |
| 030 | 50.70 | 1.801 | 1.801 | 10 | 114 | 49.43 | 1.844 | 22 |
| 320 | 60.40 | 1.533 | 1.535 | 20 | 120 | 60.44 | 1.532 | 10 |
| 302 | 61.65 | 1.504 | 1.503 | 22 | 211 | 61.40 | 1.510 | 12 |

angle, it was found that $\beta$ decreases as the hydrogen stoichiometry increases. Although orthorhombic distortions to the original $MoSi_2$-type structure were observed for $Ti_2PdH_x$ [3], $Ti_2CuH_x$ [5, 6] and $Zr_2PdH_x$ [9], these samples all had hydrogen contents with $x<4$, in contrast to $Zr_2CuH_{4.2}$.

The X-ray diffraction data for the $Zr_2CuH_{4.2}$ sample are compared in Table 2 with the peaks that had previously been obtained [9] from $Zr_2PdH_{3.4}$, which possesses an orthorhombic unit cell derived from the original tetragonal C11b structures of both $Zr_2Cu$ and $Zr_2Pd$ [4]. Although the patterns are quite similar, very different Miller indices are needed in order to represent the structures for the metal atoms. Figure 3 illustrates how the original tetragonal lattice of $Zr_2Cu$ can change into a monoclinic structure upon hydrogenation. For convenience, only the Cu atoms are shown in Fig. 3, where the end-centered plane of the monoclinic lattice arises from the face diagonal of the Cu atom planes of the $MoSi_2$-type unit cell. Furthermore, the $c$ axis of the monoclinic structure derives from half the tetragonal $c$

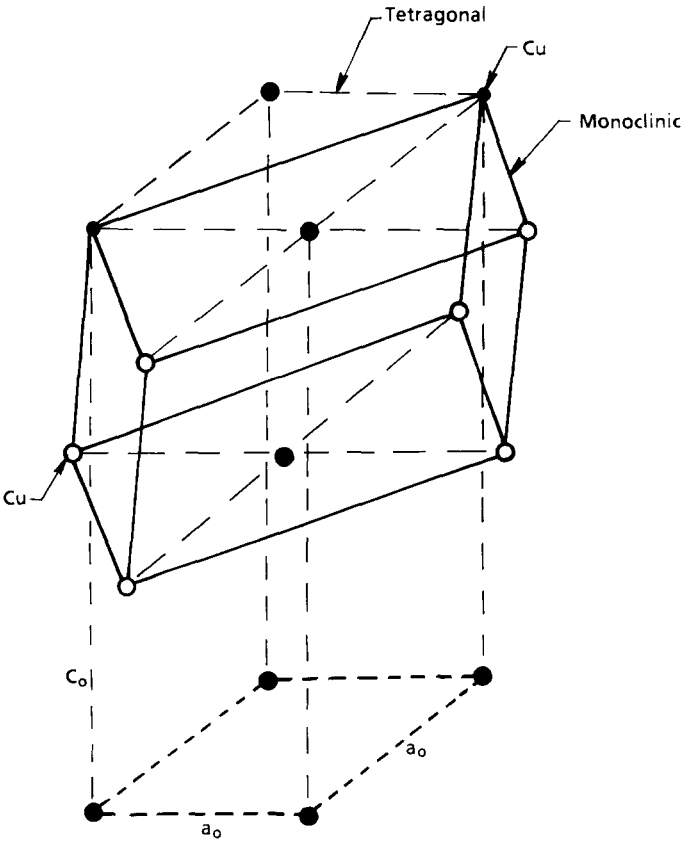


Fig. 3. Locations of Cu atoms that show both the tetragonal structure for the $Zr_2Cu$ intermetallic and the monoclinic structure for $Zr_2CuH_{4.2}$. The open circles represent Cu atoms from adjacent unit cells of the original tetragonal lattice.

axis, but it is now tilted (*i.e.* to produce the $\beta$ angle) so that the body-centered Cu atom of the original $MoSi_2$ unit cell becomes an end-centered atom of the monoclinic hydride structure. The close similarity of XRD patterns for the monoclinic and orthorhombic unit cells in Table 2 is due to only relatively small motions of the host metal atoms to accommodate the H atoms. Unfortunately, the hydrogen locations in $Zr_2PdH_{3.4}$ and $Zr_2CuH_{4.2}$ cannot be deduced from their XRD patterns. However, the proton second moments for several orthorhombic $Zr_2PdH_x$ samples with $x \approx 3$ indicated [9] that hydrogen primarily occupies the $T_a$ and $O_b$ sites in this phase. The powder neutron diffraction pattern obtained from $Zr_2CuD_{4.4}$, which will be reported in detail elsewhere [16], gave very similar unit cell parameters as well as the same Bravais lattice and probable space group that we have found by XRD for $Zr_2CuH_{4.2}$. Although a final refinement of the $Zr_2CuD_{4.4}$ crystal structure has not been obtained, preliminary evaluation of the neutron pattern for $Zr_2CuD_{4.4}$ indicates that deuterium primarily occupies four different sites of greatly distorted tetrahedral symmetry with two to four Zr atoms as nearest neighbors.

## 4. Nuclear magnetic resonance studies

The proton free-induction decay obtained from $Zr_2CuH_{4.2}$ at room temperature indicated that little hydrogen motion was present. The magnetization recoveries for the spin–lattice relaxation times ($T_1$) were exponential as expected from single-phase material. The $T_1$ data followed the Korringa relation

$$T_1T = C_k \tag{1}$$

over the temperature range 97–295 K. As described in the reviews by Cotts [17] and Bowman [18], the quantity $(T_1T)^{-1/2}$ is directly proportional to the density of electronic states at the Fermi level. However, the simultaneous contributions of several hyperfine interactions with the s and d electron states generally limit quantitative assessments [17, 18] of the specific Fermi level state densities from only the $(T_1T)^{-1/2}$ parameters. Nevertheless, eqn. (1) is useful for estimating trends in relative densities at the proton sites in different hydride phases if the hyperfine interactions predominantly arise from a common host metal. For $Zr_2CuH_{4.2}$, $(T_1T)^{-1/2} = 0.063(2)$ s K, which is between the values 0.04–0.05 s K and 0.08(1) s K obtained [18] from $ZrH_x$ and $Zr_2PdH_x$ respectively. These results are reasonable since comparisons [19] of valence band photoelectron spectra and calculated energy band state densities for $Zr_{1-y}Cu_y$ and $Zr_{1-y}Pd_y$ alloys placed their Fermi levels in states derived mainly from the zirconium d electron states.

In order to gain some insight on the hydrogen diffusion properties of $Zr_2CuH_{4.2}$, the proton $T_{1\rho}$ relaxation times were measured between 200 and 500 K. The results are presented in Fig. 4, where a minimum is observed

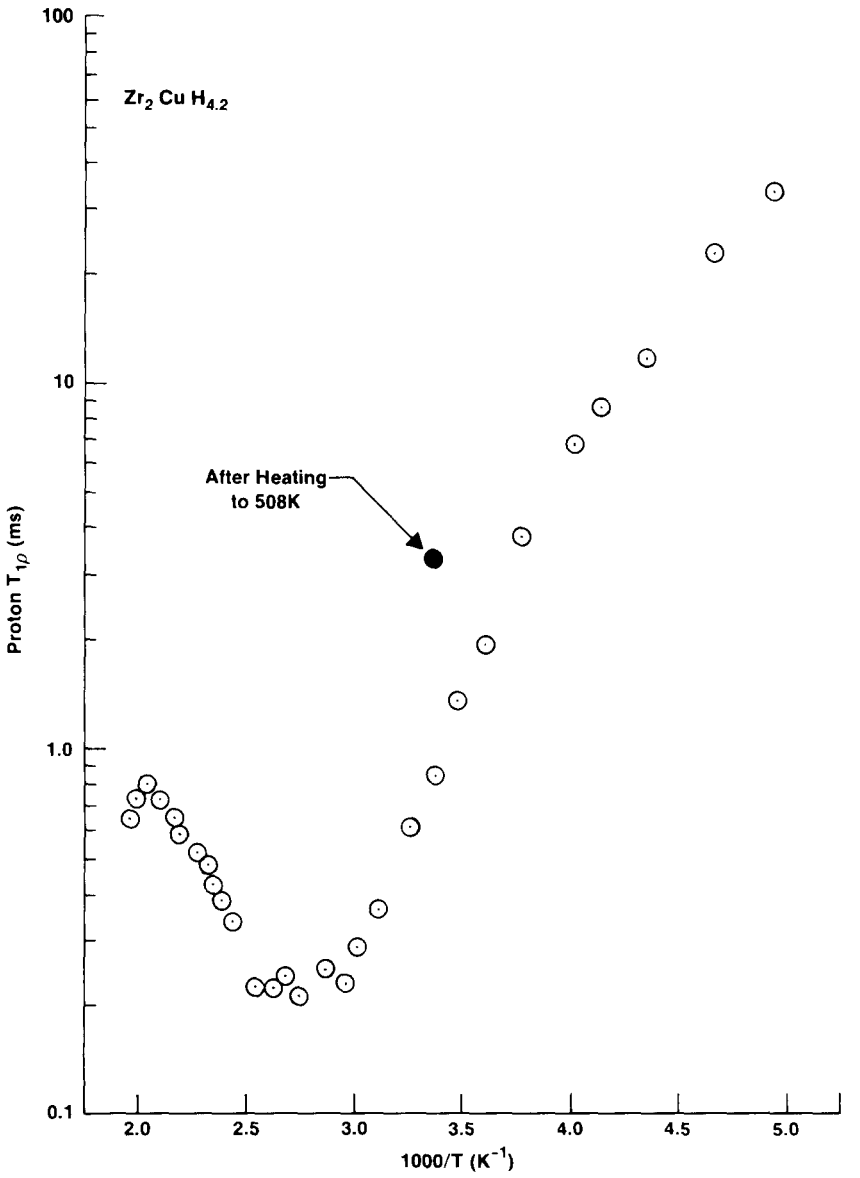


Fig. 4. Proton rotating frame relaxation times measured for $Zr_2CuH_{4.2}$.

near 365 K. The well-known [17, 18] Bloembergen–Purcell–Pound model was used to deduce the diffusion correlation times ($\tau_c$) from the $T_{1\rho}$ data. The proton-hopping rate $\tau_c^{-1}$ is plotted in Fig. 5, where an Arrhenius line with an activation energy $E_a$ of 0.28(2) eV provides a good fit between 240 and 475 K. Figure 5 also shows the Arrhenius lines and $E_a$ values previously deduced from proton $T_{1\rho}$ measurements on $Ti_2CuH_{1.9}$ [5], $Ti_2PdH_{1.9}$ [7] and

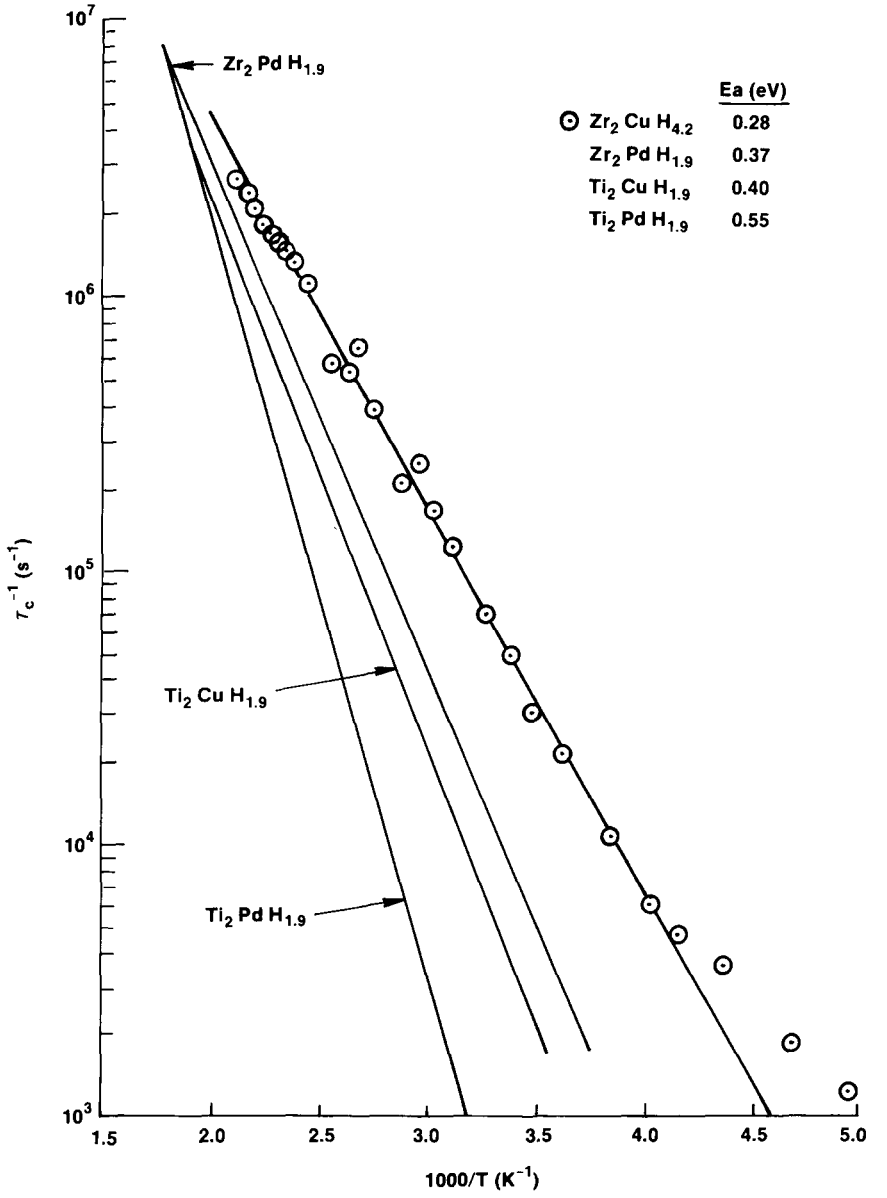


Fig. 5. Diffusion correlation times from BPP model analyses of rotating frame relaxation times.

$Zr_2PdH_{1.9}$ [8]. The H atoms are clearly more mobile (with corresponding smaller activation energy) in $Zr_2CuH_{4.2}$ than in the other three hydrides. Since H atoms predominantly occupy only the $A_4$-type sites in those hydrides with $x<2$, the occupancy of several types of sites [16] in the $Zr_2CuH_{4.2}$ structure is responsible for the increased diffusion rate.

## 5. Thermal stability

As shown in Fig. 4, heating the $Zr_2CuH_{4.2}$ sample above 480 K led to an unusual decrease in the proton $T_{1\rho}$ relaxation times with increasing temperature. Furthermore, when $T_{1\rho}$ at 300 K was remeasured, it was substantially longer than the value originally obtained prior to heating. From earlier NMR studies on $Ti_yCuH_x$ [5], these results indicate that the material had undergone a transformation. Figure 6 shows the X-ray pattern obtained from a portion of the NMR sample after heating to 508 K in the sealed tube. When compared with the XRD results in Fig. 2 for the unheated material, a substantial change is noted. The X-ray pattern for the heated material is consistent with the presence of $ZrH_x$ by the strong peak at the $2\theta$ position of 31.5° (which corresponds directly to a unique line in ICDD pattern [20] number 17-314 for $ZrH_x$) and metallic copper by the $2\theta$ peak at 43.2° as given in ICDD [20] pattern number 4-0836. Thus the presence of $ZrH_x$ and copper metal is unmistakable in the XRD pattern for the heated $Zr_2CuH_{4.2}$ NMR sample. Systematic comparison with the original pattern suggests that most of the additional broad peaks in Fig. 6 arise from a lower stoichiometry $Zr_2CuH_x$ phase with a smaller unit cell volume. However, these broad lines can also have contributions from copper-rich intermetallic phases such as hexagonal $ZrCu_{3.65}$ as described by Kadel and Weiss [2]. While the occurrence of these latter phases cannot be definitely established from the pattern in Fig. 6, the copper-rich intermetallics have strong diffraction lines lying in many of the same $2\theta$ locations as the broad peaks and their presence

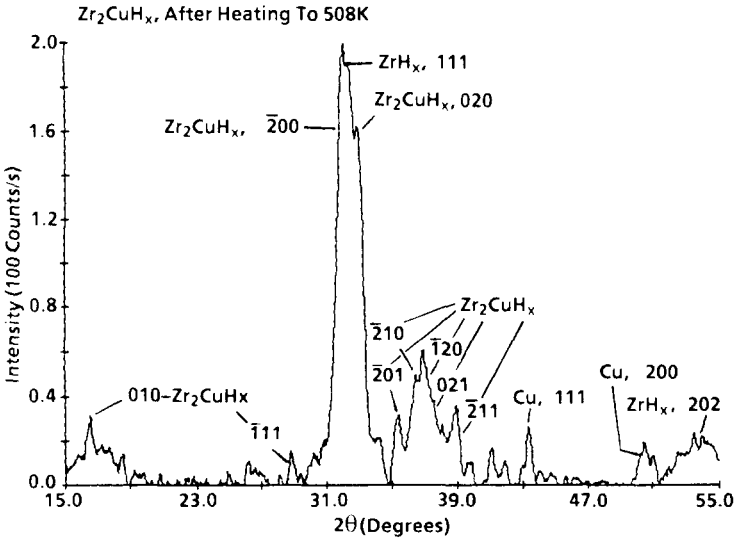


Fig. 6. X-ray diffraction pattern obtained after heating $Zr_2CuH_{4.2}$ to 500 K during NMR measurements.

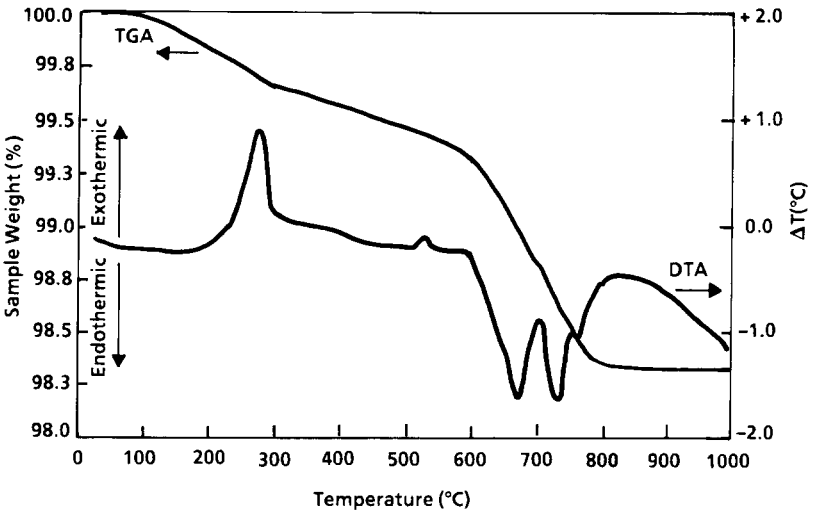


Fig. 7. Differential thermal analysis traces for $Zr_2CuH_{4.2}$ heated at rate of 10 K $min^{-1}$ under flowing helium gas.

should not be excluded. Consequently, the ternary $Zr_2CuH_{4.2}$ phase is metastable with a rather low decomposition temperature similar to those previously found for the $Ti_yCuH_x$ phases [5, 6]. Additional information on the thermal decomposition of $Zr_2CuH_{4.2}$ is provided by the thermogravimetric and differential thermal analysis curves shown in Fig. 7. This sample was heated in flowing helium gas (which will promote the loss of hydrogen in contrast to heating the hydride in a sealed NMR tube) at a rate of 10 K $min^{-1}$. Above 370 K some hydrogen starts to evolve until about 20% was released by the maximum of a rather sharp exothermic transition at 550 K. However, most of the hydrogen was released above 870 K, which was from the degassing of the decomposition product $ZrH_x$ as well as remaining $ZrCu_yH_x$ phases. The general behavior of $Zr_2CuH_{4.2}$ is quite similar to that previously seen [6] for $Ti_2CuH_x$ – including the occurrence of an exothermic transition below 600 K. However, the greater hydrogen content in $Zr_2CuH_{4.2}$ requires occupancy in several less stable sites, which has led to hydrogen evolution at lower temperatures and somewhat greater tendency towards decomposition than had been observed [5, 6] for the $Ti_yCuH_x$ samples.

## 6. Conclusions

X-ray and NMR studies of $Zr_2CuH_{4.2}$ revealed several similarities to the behavior previously seen in the related $Ti_2PdH_x$, $Ti_2CuH_x$ and $Zr_2PdH_x$ systems. However, $Zr_2Cu$ can accommodate hydrogen in more types of interstitial sites, leading to a different crystal structure (*i.e.* monoclinic *vs.* orthorhombic) as well as enhanced hydrogen mobility and reduced thermal stability.

## Acknowledgment

EG&G Mound Applied Technologies is operated for the US Department of Energy under Contract DE-AC04-88DP43495.

## References

1 A. J. Maeland, *J. Less-Common Met.*, *89* (1983) 173.
2 R. Kadel and A. Weiss, *J. Less-Common Met.*, *65* (1979) 89.
3 R. Kadel and A. Weiss, *Ber. Bunsenges. Phys. Chem.*, *82* (1978) 1290.
4 A. J. Maeland and G. G. Libowitz, *J. Less-Common Met.*, *74* (1980) 295.
5 R. C. Bowman Jr., A. J. Maeland and W. K. Rhim, *Phys. Rev. B*, *26* (1982) 6362.
6 R. J. Furlan, G. Bambakidis, J. S. Cantrell, R. C. Bowman Jr. and A. J. Maeland, *J. Less-Common Met.*, *116* (1986) 375.
7 R. C. Bowman Jr., A. Attalla, G. C. Abell, A. J. Maeland and J. S. Cantrell, *J. Less-Common Met.*, *172–174* (1991) 643.
8 R. C. Bowman Jr., A. Attalla, A. J. Maeland and W. L. Johnson, *Solid State Commun.*, *47* (1983) 779.
9 F. E. Spada, R. C. Bowman Jr. and J. S. Cantrell, *J. Less-Common Met.*, *129* (1987) 197.
10 R. C. Bowman Jr., D. R. Torgeson, R. G. Barnes, A. J. Maeland and J. J. Rush, *Z. Phys. Chem. N.F.*, *163* (1989) 425.
11 M. V. Nevitt, in J. H. Westbrook (ed.), *Intermetallic Compounds*, Wiley, New York, 1967, pp. 214–229.
12 R. P. Goehner, in J. R. Rhodes, C. S. Barrett, D. E. Leyden, J. B. Newkirt, P. K. Predecki and C. O. Rudd (eds.), *Advances in X-ray Analysis*, Vol. 23, Plenum, New York, 1980, pp. 305–311.
13 Program *Lattice*, adapted by E. F. Jendrek (EG&G Mound) from a program originally written by D. E. Appleman and H. T. Evans, *USGS-GD-73-003*, US Geological Survey Report, Washington, DC, 1973.
14 A. J. Maeland, E. Lukacevic, J. J. Rush and A. Santoro, *J. Less-Common Met.*, *129* (1987) 77.
15 A. F. Andresen and A. J. Maeland, *J. Less-Common Met.*, *129* (1987) 115.
16 A. F. Andresen and A. J. Maeland, unpublished results, 1991.
17 R. M. Cotts, in G. Alefeld and J. Volkl (eds.), *Hydrogen in Metals I: Basic Properties*, Springer, Berlin, 1978, p. 227.
18 R. C. Bowman Jr., *Hyperfine Interact.*, *24–26* (1985) 583.
19 V. L. Morruzzi, P. Oelhafen, A. R. Williams, R. Lapka, H.-J. Guntherodt and J. Kubler, *Phys. Rev. B*, *27* (1983) 2049.
20 JCPDS, International Center for Diffraction Data, 1601 Park Lane Swarthmore, PA 19801, USA.